RESEARCH PAPER

The Structural, Morphological, Optical and Photoluminescence Studies of Mn^{2+} Doped $CdS/Zn_3(PO_4)_2$ Nanocomposites

Gogula Sreedevi[1], Kanakala.Venkata Rao[2,5], Gogula. Jaya Ram Pavan Kumar [3], B.Tirumala Rao[4], Sandhya Cole[5,*]

** g.sridevimsc@gmail.com*

[1] Dept. of Physics, P.V.P. Siddhartha Institute of Technology, Vijayawada, A.P., India
[2] Dept. of Physics, Government Polytechnic, Krosuru, Guntur, A.P., India
[3] Dept. of H&S, Andhra Engineering College, Atmakur, Nellore, Andhra Pradesh
[4] Dept. of Physics, Vishnu Institute of Technology, Bhimavaram, A.P., India
[5] Dept. of Physics, Acharya Nagarjuna University, Nagarjuna Nagar, A.P., India

Received: November 2021 **Revised: June 2022** **Accepted: August 2022**
DOI: 10.22068/ijmse.2574

Abstract: *The present study used a hydrothermal technique to synthesize undoped and Mn^{2+} doped $CdS/Zn_3(PO_4)_2$ semiconducting nanocomposite materials. Powder X-ray diffraction, scanning electron microscopy, UV-Vis diffuse reflectance spectrometer, Fourier transform-Infrared Spectroscopy-FT-IR, and photoluminescence techniques were employed to study structural, optical, and luminescence properties of produced nanocomposites. The hexagonal structure of CdS and the monoclinic structure of $Zn_3(PO_4)_2$ are both reflected in the powder X-ray diffraction spectra. When Mn^{2+} ions are present in the host lattice, a lattice distortion occurs, causing a phase change from the phase of γ-$Zn_3(PO_4)_2$ to the β-phase of $Zn_3(PO_4)_2$, without affecting the hexagonal phase of CdS. The average crystallite size of produced nanocomposites was 22-25 nm, and also calculated the lattice strain and dislocation density to better understand internal deformation of the samples. The FT-IR spectra were used to investigate the molecular vibrations and functional groups in the samples. The surface morphology of the nanocomposites is hexagonal spheres on rectangular shaped nano-flakes, and the interatomic distance between the hexagonal spheres is decreased as the doping concentration increases, forming a rod-like structure on the flakes. EDAX results confirm the presence of various relevant elements in the prepared samples. The quantum confinement of produced samples reduces as the Mn^{2+} doping concentration in the host lattice increases. The photoluminescence results demonstrate shallow trapped states due to the transition: d-d ($^4T_1 \rightarrow {}^6A_1$) of the tetrahedrally coordinated Mn^{2+} states and the impact of Mn^{2+} ions exhibiting several peaks in the UV-Visible region (365-634 nm) generating RGB (Red, Green, Blue) luminescence. Color coordinates and CCT values were calculated using the CIE diagram, and color correlated temperatures in the range of 2513–7307 K were discovered, which might be used in solid state lighting applications.*

Keywords: *Photoluminescence; CdS; Nanocomposite; $Zn_3(PO_4)_2$; Mn^{2+}*

1. INTRODUCTION

Electronic technology in the present period focuses on the development of new functional materials and the application of scientific knowledge of electronics to the design of novel devices in order to provide a flexible, sustainable, and technologically beneficial environment for mankind Semiconducting materials provide the foundation for contemporary electronics, which include solid-state devices, transistors, and integrated circuits enabling the development of electronic-communication systems and security systems. Because of their broad size dependant features, tiny dimensional semiconductors are generating a lot of attention among fundamental scientific, technical, and industrial researchers these days. Because of the increased surface area to volume ratio and quantum confinement effect, semiconducting materials' structural and optical characteristics change dramatically when their size shrinks to the nanoscale [1]. Nano semiconducting materials are already being used to forecast new features and applications in a variety of industries. Nanocomposite semiconductors, which are made up of two or more separate component materials, are frequently utilized in electronic technology to change structural, electrical, and optical characteristics. Nanocomposites are multiphase materials with higher thermal stability and catalytic activity than single-phase materials.

Phosphates are now used as host-lattices in the development of innovative opto-electronic functional materials. In terms of possible applications, the growth of phosphor industry is

aided by the development of novel phosphor materials triggered by transition metal ions or rare earth ions. Cadmium sulfide/Zinc phosphate are active materials that are extensively utilized as hosts for luminescent applications such as light emitting diodes, solid state lighting, display devices, solar cells, sensors, and biomedical applications. Furthermore, it is widely known that cadmium sulfide (CdS) has sparked a lot of attention among many inorganic semiconductors due to its quantized energy levels, size dependant characteristics, configurable bandgap, and chemical stability. CdS is a semiconductor with an indirect bandgap of 2.42 eV. It was used in numerous optoelectronic and luminescence applications such as light emitting diodes, solar cells, photochemical catalysis, and gas sensors due to its outstanding photo absorption capabilities [2]. Zincphosphate ($Zn_3(PO_4)_2$) is a common white inorganic, non-toxic, multi-functional semiconductor with corrosion resistance and sticky properties. It may be utilized as dental cement and chemically bonded ceramic (CBC) material due to its limited solubility in water and biological environments. Because of its large energy bandgap, $Zn_3(PO_4)_2$ is employed as a host lattice for luminescent, optical communications and display devices [3].

Due to its partly filled d-orbital, the transition metal ion Mn^{2+} doped into $CdS/Zn_3(PO_4)_2$ nanocomposites exhibits unique catalytic, electrical, optical and magnetic characteristics, and is a well-known phosphor in cathode tubes [4]. The hydrothermal approach for producing nanophosphors is a simple and adaptable process that produces nanoparticles with highly regulated size and shape. The present investigation aims at finding out the influence of Mn^{2+} ions on the structural and spectral properties of $CdS/Zn_3(PO_4)_2$ nanocomposite powders prepared by hydrothermal method and analyzed by using powder X-ray Diffraction (XRD), FT-IR-Fourier Transform Infrared spectroscopy, SEM-Scanning Electron Microscopy with Energy Dispersive X-ray (EDAX), UV-Vis Spectroscopy (DRS), Photoluminescence (PL) with CIE-diagram techniques.

2. EXPERIMENTAL PROCEDURES

2.1. Materials

Cadmium nitrate tetrahydrate ($Cd(NO_3)_2.4H_2O$), Thiourea (CH_4N_2S), Zinc phosphate ($Zn_3(PO_4)_2$), and maganesoxide (MnO) were purchased as precursor materials with analytical grade purity (>99 percent) from Merck chemicals, Mumbai, India, to synthesize $CdSZn_3(PO_4)_2$-undoped and $CdSZn_3(PO_4)_2$-(0.3, 0.6, and 0.9 mol %) Mn^{2+} ions doped nanocomposites under hydrothermal method. De-ionized water was employed as a solvent to make the solution. To prevent contaminants, glassware used in the process was cleansed many times with distilled water.

2.2. Composite Preparation

The appropriate molar amounts of ($Cd(NO_3)_2.4H_2O$), (CH_4N_2S), $Zn_3(PO_4)_2$ and MnO were dissolved in 60 ml deionised water and 20 ml ethanol in a conical flask and the mixture was stirred continuously with a magnetic stirrer for 2 hours at room temperature according to stoichiometric ratio. During the stirring process, 0.025 mol percent NaOH is slowly added to the prepared solution to obtain a transparent solution without aggolemarization, and the solution is stirred continuously with a magnetic stirrer at room temperature for two hours, after which the solution turns dark yellow, indicating the incorporation of Mn^{2+} ions into $CdS(Zn_3PO_4)_2$ nanocomposite. To generate a high-quality crystalline product, the prepared solution was put into a 150 ml Teflon-coated autoclave and heated to 100^{o}C for three hours. After cooling to room temperature the produced solution, was washed multiple times with distilled water to remove contaminants, filtered and then dried for a duration of 6 hours at 60^{o}C. Finally, the synthesized samples are well grinded. The chemical composition of samples synthesized with different molar percentages of dopant element (MnO) is given below

Mn_0: 40% $Zn_3(PO_4)_2$ + 60.0% ($Cd(NO_3)_2.4H_2O$ + CH_4N_2S)

Mn_1: 40% $Zn_3(PO_4)_2$ + 59.7% ($Cd(NO_3)_2.4H_2O$ + CH_4N_2S) + 0.3% MnO

Mn_2: 40% $Zn_3(PO_4)_2$ + 59.4% ($Cd(NO_3)_2.4H_2O$ + CH_4N_2S) + 0.6% MnO

Mn_3: 40% $Zn_3(PO_4)_2$ + 59.1% ($Cd(NO_3)_2.4H_20$ + CH_4N_2S) + 0.9% MnO

2.3. Characterization and Analytical Techniques

Powder X-ray diffraction patterns were recorded using PAN analytical, X' Pert model in the scanning range of 20^o– 90^o, using Cu-kα radiation

(λ= 1.5406 Å), and peak position, intensity, crystalline phases, and crystalline size of prepared samples were examined using X' Pert Pro software. FT-IR spectra were used to investigate the bonding mechanism and molecular vibrations of produced nanocomposites. SHIMADUZU-IR, Affinity-1S FT-IR spectrophotometer is used to measure FT-IR spectra in the middle infrared band (400-4000 cm^{-1}) at room temperature. Scanning electron microscopy (SEM; TESCAN, VEGA3 LMU model) with an accelerating voltage of 15 KV was used to acquire high resolution three dimensional surface morphology and chemical composition of produced MnO doped $CdSZn_3(PO_4)_2$ composites by acquisition of EDAX. SPECORD-210 plus, Analytic Jena diffused reflectance spectrophotometer in UV-Vis (300- 1000 nm) range was used to record the diffuse reflectance spectra of the prepared samples and the reflection data of the obtained spectra was converted into the absorbance data using the Kubelka Munk relation to estimate the optical band gap energy of the prepared samples. Xenon lamp equipped PERKIN ELMER LS-55 spectrometer was used to record Photoluminescence spectra at excitation wavelength of 325 nm to analyze the luminescence behavior of the current samples. Color chromaticity studies were carried out in order to calculate color co-ordinates and temperature correlations (CCT). All of the analytical tests were carried out at room temperature.

3. RESULTS AND DISCUSSION

3.1. Structural & Morphological Properties

3.1.1. X-ray diffraction

The powder X software was used to investigate the X-ray diffraction patterns of undoped and Mn^{2+} doped $CdSZn_3(PO_4)_2$ nanocomposites. The prepared composites are well crystallized, as seen by the strong and narrow peaks. They were all compatible with the CdS-hexagonal phase and the intermixing of γ, β-monoclinic $Zn_3(PO_4)_2$ phases. The relative intensities of the diffraction peaks of prepared samples were in good agreement with the stated standard (CdS: JC-PDS #65-3414, $Zn_3(PO_4)_2$: γ-phase JCPDS#30-1490, β-phase JCPDS #30-1489), as shown in Fig. 1.

In undoped $CdSZn_3(PO_4)_2$ sample the diffraction peaks are matched with hexagonal phase of CdS and monoclinic γ-phase of $Zn_3(PO_4)_2$.

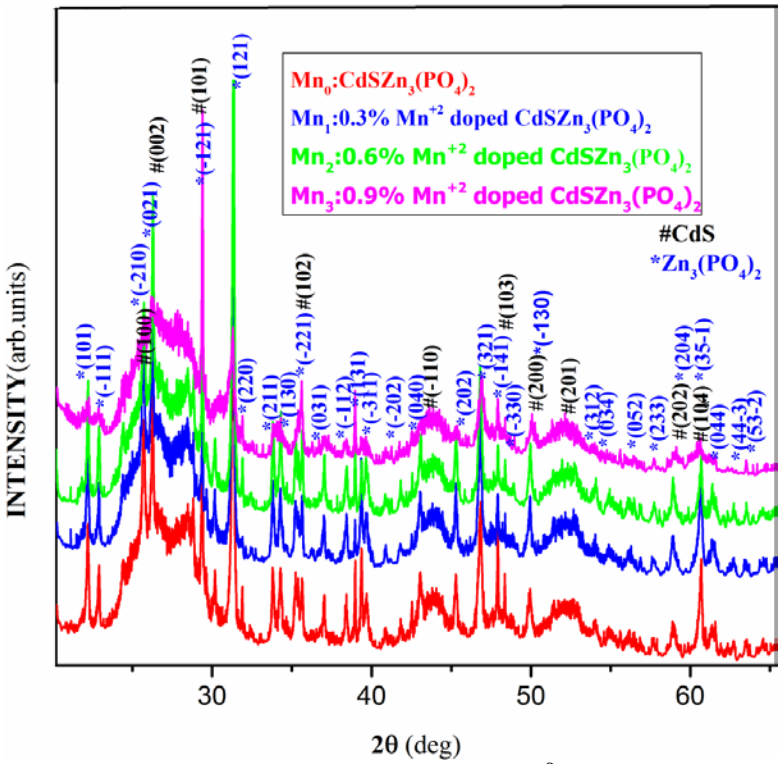

Fig. 1. XRD pattern of $CdSZn_3(PO_4)_2$ and (0.3%, 0.6% and 0.9%) Mn^{2+} doped $CdSZn_3(PO_4)_2$ nanocomposites.

With doping of Mn^{2+} ions in host lattice of $CdSZn_3(PO_4)_2$ there is a phase transformation of γ-phase of $Zn_3(PO_4)_2$ to β-phase but there is no distortion in the hexagonal phase of CdS. With increasing of Mn^{2+} doping concentration, γ-phase peaks intensity found to decreases and β-phase peaks intensity increases. In Mn^{2+} doped samples there is a small deviation in the peak positions towards the higher angle which results from the fact that Cd^{2+}, Zn ions substituted by Mn^{2+} ions in the host lattice causing variations of lattice parameters indicates the lattice distortion. [5-7].

The dopant cannot create a separate peak by the side of the host peak, according to Vegard's law [1], but it can have a little modification in the peak positions of the host lattice. Due to its smaller ionic radius (0.66 A°) than CdS (0.97 A°) and Zincphosphate (0.74 A°), it was deduced that the host lattice could contain Mn^{2+} ions. Furthermore, the electro negativities of Mn, Cd, and Zn cations are 1.55, 1.69, and 1.65, respectively, which differ from sulfur (2.58), implying that Mn^{2+} ions most likely incorporate into the host-lattice at vacancy sites. The presence of Mn^{2+} ions in the host lattice causes distortion in the lattice, which is represented by lattice strain and implies a little modification in the lattice parameters. The change over of the γ-phase of $Zn_3(PO_4)_2$ to the β-$Zn_3(PO_4)_2$ phase, as well as their related lattice parameter values, has been seen as the doping concentration of Mn^{2+} ions increases.

Table 1 (a&b) shows the lattice parameters calculated from the XRD pattern, these values are had good correlation with the conventional JCPDS values.

Debye-Scherrer's formula is used to calculate the average size of crystallites, as follow:

$$D = \frac{k\lambda}{\beta\cos\theta}$$

Where in this formula kis the shape dependent factor, D is the average size of crystal lattice, λ=1.5406 Å, denotes the Cu-kα X-ray radiation's wavelength, β is taken in radians and is the full width at half maximum-FWHM of X-ray diffraction peaks, and θ denotes Bragg's diffraction angle.

Stress is not taken into account in Debye-Scherrer's equation for calculating crystallite size, hence particles are regarded stress-free. Stokes-Wilson equation is employed to calculate induced strain [6],

$$\varepsilon = \frac{\beta}{4\tan\theta}$$

Williamson and Hall (W-H) plot technique is used to calculate average crystal lattice size and micro strain, which requires de-convolution of both induced size and strain broadening by measuring the width of the peak as a function of 2θ W-H equation is expressed as:

$$\beta\cos\theta = (0.9\,\lambda/D) + 4\varepsilon\sin\theta$$

Uniform strain is assumed in all crystallographic directions in the preceding equation.

For Mn_0, Mn_1, Mn_2, and Mn_3 samples, 4 sinθ along the x-axis and β cosθ along the y-axis are shown, as shown in Fig. 2.

Table 1. Phase, Lattice parameters, volume of unit cell and Axes of symmetry of X-ray diffraction patterns of pure $CdSZn_3(PO_4)_2$ and Mn^{2+} doped $CdSZn_3(PO_4)_2$ nanocomposites.

		CdS				
Sample code	**Phase**	**Lattice Parameters (Å)**			**Volume of Unit cell**	**Axes of symmetry**
		a	b	c	($3a^2c/2$)	α= β= 90º and γ
Mn_0	Hexagonal	4.123	4.123	6.82	173.9	119.97º
Mn_1	Hexagonal	4.128	4.128	6.76	172.7	119.65º
Mn_2	Hexagonal	4.125	4.125	6.72	171.5	119.66º
Mn_3	Hexagonal	4.134	4.134	6.78	173.8	119.79º
JCPDS(65-3414)		4.132	4.132	6.73	172.35	120º
		$Zn_3(PO_4)_2$				
Sample code	**Phase**	**Lattice Parameters (Å)**			**Volume of Unit cell**	**Axes of symmetry**
		a	b	c	Sinβ(abc)	α= γ= 90º and β
Mn_0	γ, β Mixed state	7.549	8.499	5.04	320	108.03º
Mn_1	γ, β Mixed state	7.89	8.88	8.07	532.84	109.54º
Mn_2	γ, β Mixed state	8.76	7.98	8.12	530.45	110.85º
Mn_3	β-$Zn_3(PO_4)_2$	9.74	8.153	8.18	603.20	111.78º
JCPDS(30-1489)		9.175	8.26	8.86	607	112.80º
JCPDS(30-1490)		7.549	8.499	5.04	322	95.03º

From slope and intercept, micro strain and crystallite size are calculated respectively, using a straight line fit of the data. The existence of dislocation density (the length of dislocation lines/unit volume) has been shown to have a significant effect on the material's characteristics. The formula for dislocation density $\delta=1/D^2$ is also used to compute the dislocation density. The crystallite size, microstrain and dislocation density as determined by Debye-and Scherer's and W-H plots, are tabulated as Table 2. With doping of Mn^{2+} ions there is a slight enhancement in size of crystallite. It has also been noticed that the microstrain and dislocation density decreases with increase of grain size and is in good accordance with earlier report [8, 9]. Lattice strain and dislocation density values are found to decrease with increasing size of crystallite due to increase in dopant concentration.

3.1.2. Fourier Transform infrared (FT-IR)

To investigate internal order of materials like nanocomposites infrared spectroscopy is a versatile, very sensitive and most commonly used technique. The FTIR spectra gives complete information about the molecular vibrations as well as rotations associated with a covalent bond. Due to change in the dipole moment of the molecule it possesses IR spectra and involves the twisting, bending, rotating and vibrational motions in a molecule.

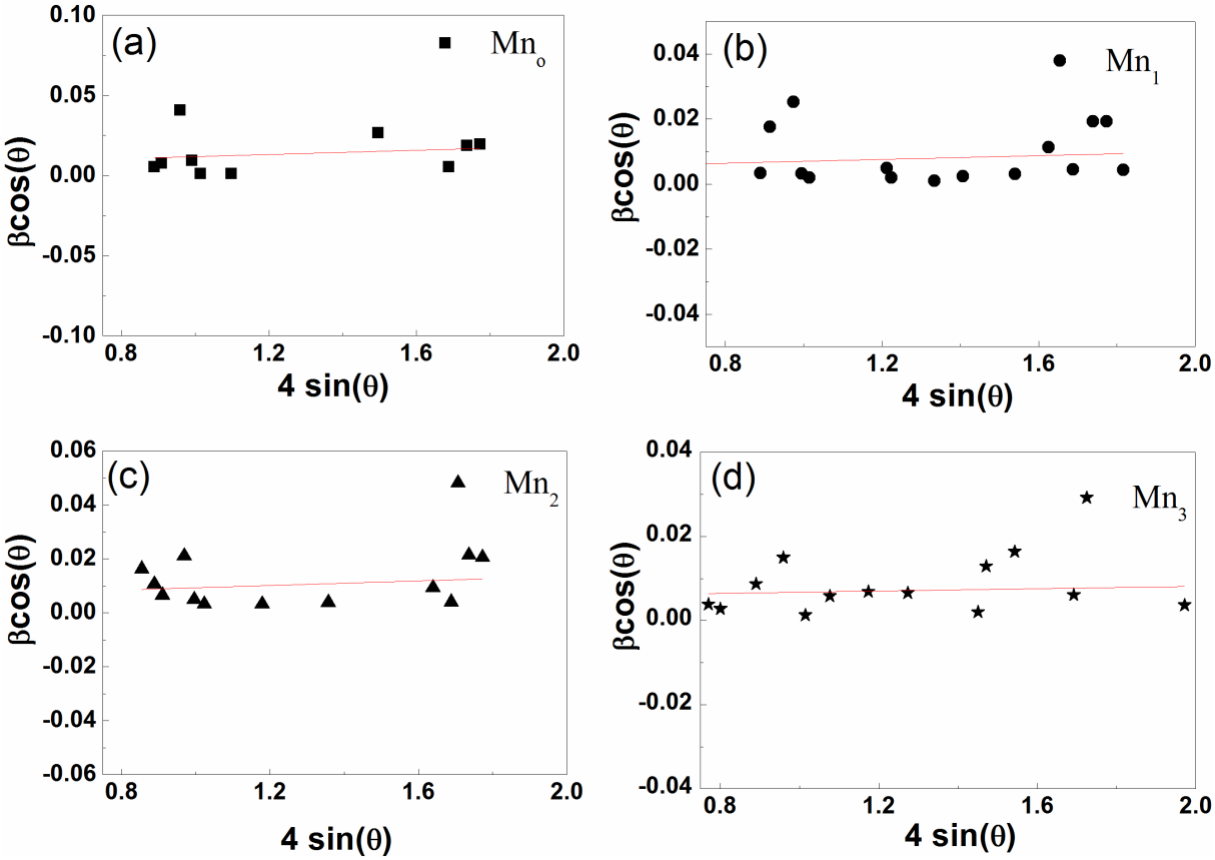

Fig. 2. W-H plot of $CdSZn_3(PO_4)_2$ and (0.3%, 0.6% and 0.9%) Mn^{2+} doped $CdSZn_3(PO_4)_2$ nanocomposites.

Table 2. caluculation of average crystallite size, lattice strain and dislocation density of $CdSZn_3(PO_4)_2$ and Mn^{2+} doped $CdSZn_3(PO_4)_2$ from Debye-Scherrer and W-H plot.

Sample Code	Crystallite size (nm)		Lattice strain ($\varepsilon \times 10^{-4}$)		Dislocation density ($\delta \times 10^{15}$ m^{-2})	
	Scherrers	W-H plot	Scherrers	W-H plot	Scherrers	W-H plot
Mn_0	22.96	24.52	9.25	13.4	1.89	1.66
Mn_1	24.98	26.78	9.04	12.82	1.72	1.33
Mn_2	25.32	27.21	8.92	12.54	1.72	1.38
Mn_3	25.89	27.98	8.83	12.38	1.56	1.49

To identify functional groups and vibrational modes presented in undoped and Mn^{2+} doped $CdSZn_3(PO_4)_2$ nanocomposites the transmittance mode FT-IR technique is employed in the wave number range400-4000 cm^{-1} and corresponding FT-IR spectra are plotted as Fig. 3. The functional groups with corresponding wave number are represented in Table 3. By comparing undoped and Mn^{2+} doped FT-IR spectra's, it is clear that all the samples exhibit same features, but the position of peaks and intensity of the peaks were little bit changed. The important finding from this work is that when the doping concentration is increased, the peak area of O-H, C=O, and C=C increases, indicating that Mn^{2+} ions and $CdSZn_3(PO_4)_2$ nanocomposites are coordinated.

The intense interaction of water with the surface of CdS causes a broad dip at 3460 cm^{-1}. An absorption band occurs at 944 cm^{-1} due to S-O stretching vibration. The H-O-H bending mode of the adsorbed lattice water causes broad and strong peaks at 1583 cm^{-1} [10]. It refers to almost free water molecules trapped in the lattice during composite contact with the lattice.

3.1.3. Morphological studies

Scanning electron microscopic technique is employed to study the surface morphology and to identify the chemical composition of prepared nanocomposites. The morphological images of $CdSZn_3(PO_4)_2$ undoped nano composite and $CdSZn_3(PO_4)_2$ (0.3, 0.6, and 0.9 mol%) Mn^{2+} doped nanocomposites are shown in Fig. 4.

In case of undoped SEM images, it has been observed as rectangular flakes surrounded by CdS-hexagonal spheres which are non-uniformly distributed agglomerated. The narrow space between the particles causes the occurrence of large surface area agglomerations in the sample. With increasing concentration of Mn^{2+} ions doping from 0.3 to 0.9 mol%, interatomic distance between the particles decreases and bonding strength increases and forms a spherical network bonding of CdS hexagonal spheres on the rectangular flakes without agglomerations [11]. Interestingly in 0.9 mol% Mn doped sample bonding length between the particles increases and shows rod like structure on the rectangular flakes [30]. The energy dispersive X-ray spectroscopy (EDAX) measurements were carried out to determine overall elemental composition and spatial distribution of undoped and Mn^{2+} doped $CdSZn_3(PO_4)_2$ nanocomposites and their corresponding spectra are depicted in Fig. 5.

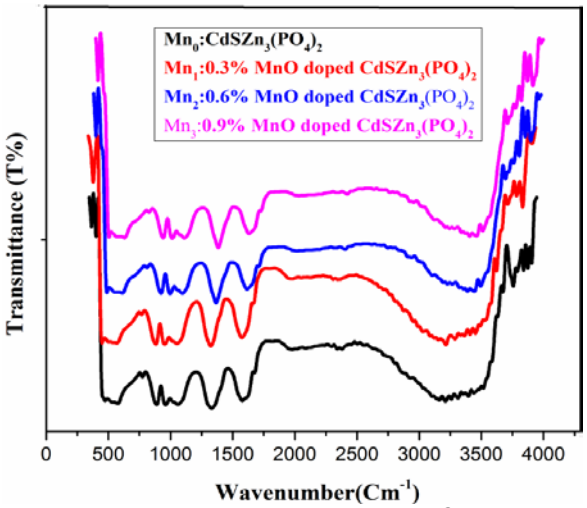

Fig. 3. FT-IR spectra of pure and Mn^{2+} doped $CdSZn_3(PO_4)_2$ nanocomposites.

Table 3. Infrared vibrational assignment of peak positions, Intensity with its corresponding frequency region for $CdSZn_3(PO_4)_2$ and (0.3, 0.6 and 0.9 mol%) Mn^{2+} doped $CdSZn_3(PO_4)_2$ nanocomposites.

Vibrational frequency				Intensity	Band assignment
Mn_0	Mn_1	Mn_2	Mn_3		
592	600	604	618	Week& broad	P–O Symmetric stretching mode
901	912	928	936	Sharp	C-H Stretching
962	971	1005	1025	Strong& broad	Asymmetric P–O stretching mode
1053	1065	1114	1134	Sharp& broad	C-O, S-O anti-symmetric
1112	1080	1050	1035	Strong	symmetric stretching of PO_4^{3-}
1372	1296	1288	1271	strong and broad	CH_3
1607	1548	1531	1523	Sharp	O-H bending vibration
1775	1725	1699	1683	broad	O-H bending vibration
2381	2331	2329	2313	Small weak	S-H BOND
3388	3355	3346	3323	Broad	Intermolecular bonds
3817	3792	3768	3749	Broad	Vibrations of O-H stretching absorbed water on the surface of the samples

The collected elemental compostions of Zn, P, O, Cd, S, Mn were shown in the inset of the Fig. 5. These collected results were in well accordance with the experimental molar ratio calculations. From the compositional analysis, it has been observed that with increasing in doping concentration of Mn^{2+} ions (from 0.3 to 0.9 mol%), the contents of Zn and O_2 are found to increase while the content of Cd is found to systematic decrease. Clearly, this is an indication of substation of Cd ions with Mn^{2+} ions.

3.2. Optical Studies

3.2.1. Diffuse reflectance spectroscopy

To monitor the optical behavior of the semiconducting nanocomposite materials an effective and important UV-Visible diffuse reflectance spectroscopy tool has been employed. The optical properties of $CdSZn_3(PO_4)_2$-undoped nanocomposite and $CdSZn_3(PO_4)_2$-(0.3, 0.6 and 0.9 mol%) Mn^{2+} doped nanocomposites are represented in Fig. 6.The optical energy bandgap of synthesized nanocomposites are estimated by using Kubelkae-Munk equation [12-13].

$$F(R) = \frac{(1-R)^2}{2R} = \frac{K}{S}$$

Where K-M function is written as function of R i.e., F(R), K denotes coefficient of absorption, S denotes coefficient of scattering, R denotes Reflectance.

A graph of K/S on y-axis versus energy on x-axis with a linear component is drawn to estimate the energy band gap. The energy band gap of nanocomposites is obtained by extrapolating the straight line to F(R)= 0.

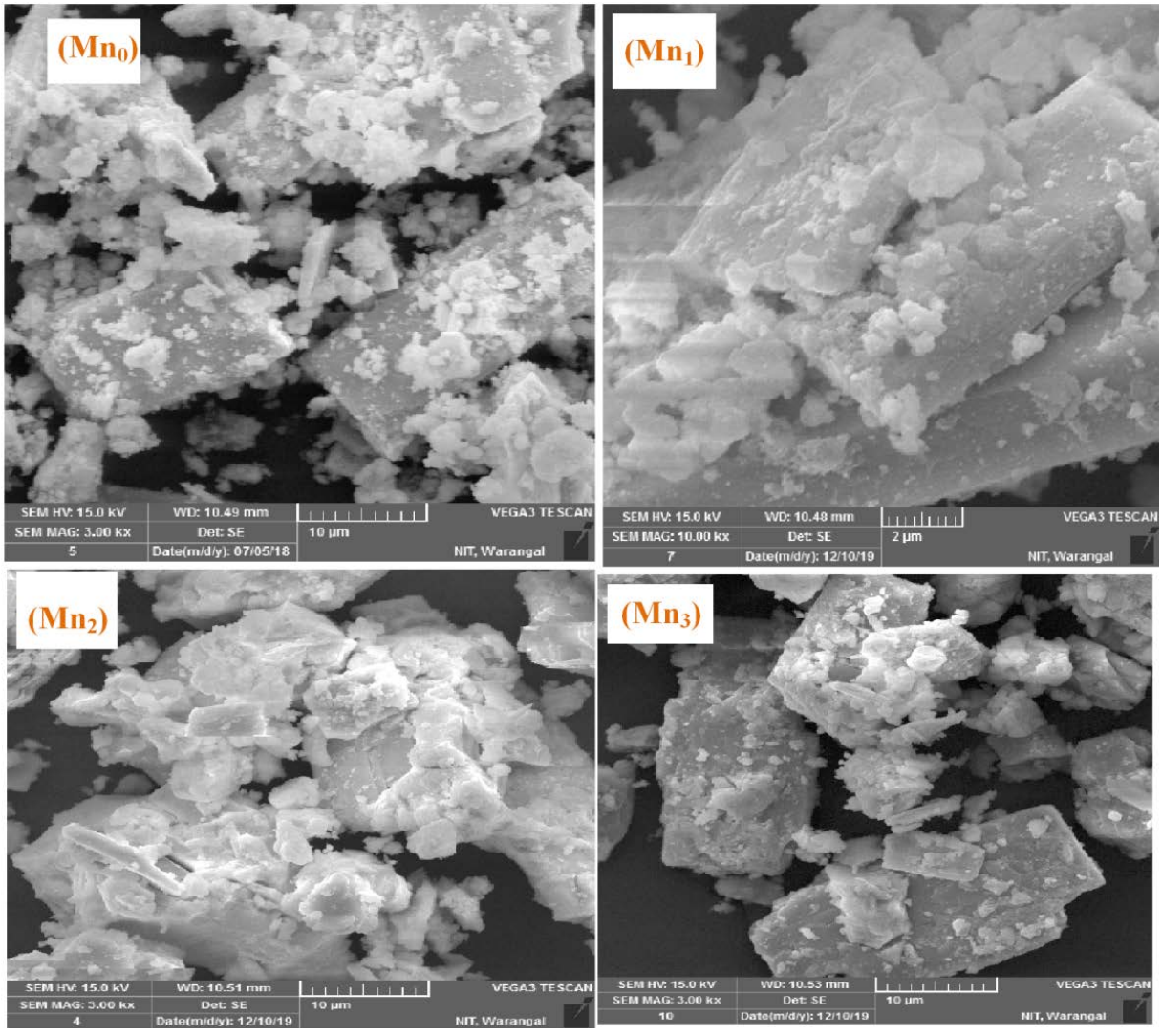

Fig. 4. SEM micrographs for the $CdSZn_3(PO_4)_2$. (Mn_0) and Mn^{2+} doped $CdSZn_3(PO_4)_2$ (Mn_1, Mn_2 and Mn_3) nanocomposites.

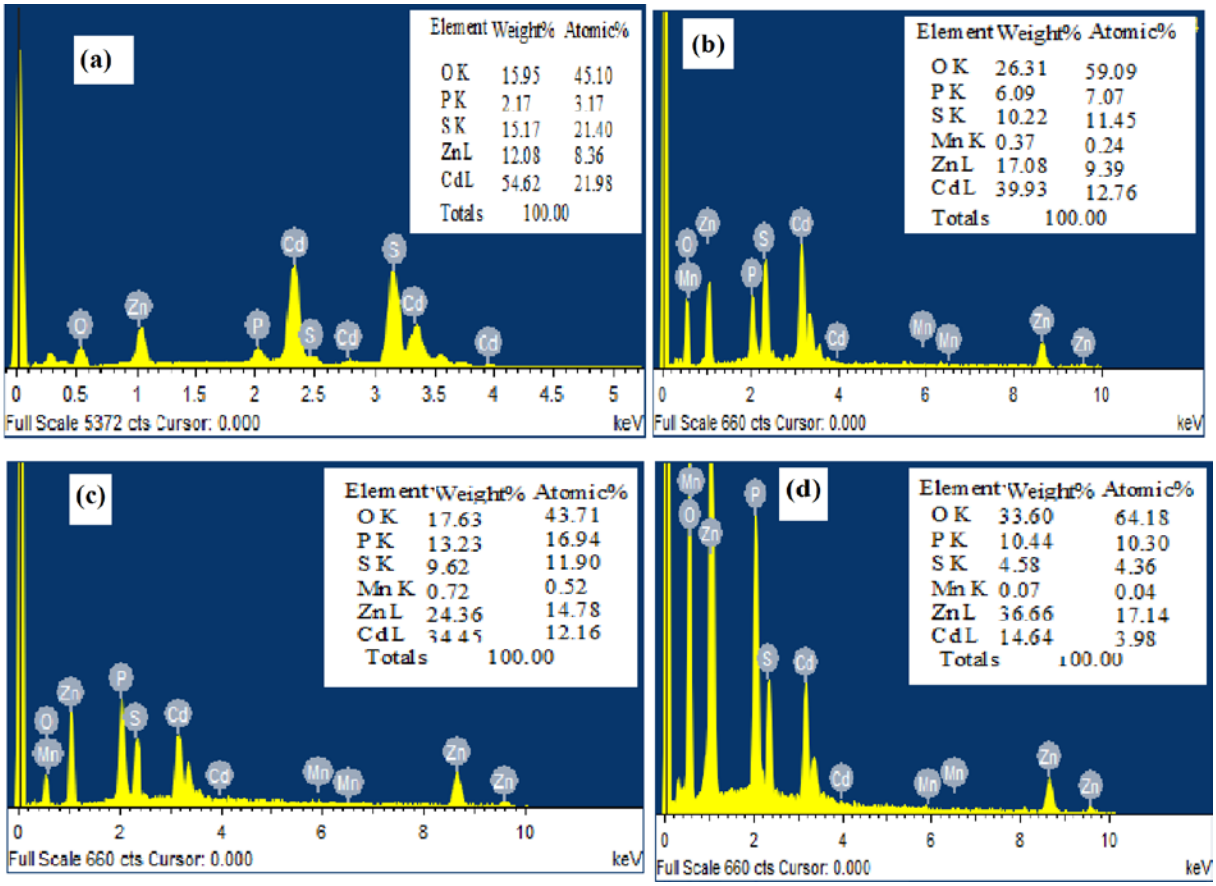

Fig. 5. EDAX Images for (a) $CdSZn_3(PO_4)_2$. (b) 0.3% (c) 0.6% and (d) 0.9% of Mn^{2+} doped $CdSZn_3(PO_4)_2$ nanocomposites.

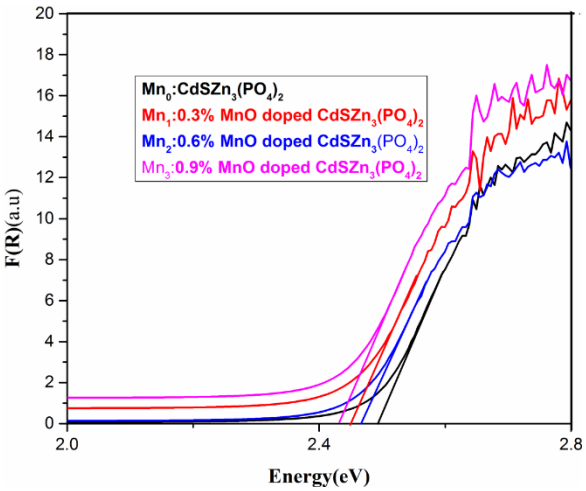

Fig. 6. UV-Vis diffuse reflectance spectra of $CdSZn_3(PO_4)_2$ and Mn^{2+} doped $CdSZn_3(PO_4)_2$ nanocomposites.

Crystallite size, local disorder, and change of band gap values are evaluated and their band gap values are given in Table 4. 4 along with dopant concentration to understand the influence of optical characteristics by the integration of Mn^{2+} ions into the host lattice of $CdS/Zn_3(PO_4)_2$.

Fig. 7 shows the measured energy band gap values, which vary from 2.48 to 2.434 eV. In the present study, it has been observed that with increasing of Mn^{2+} ions doping concentration energy bandgap decreases.

This happens due to the substitution or interstitial of Mn ions in the host lattice and in the grain boundaries there occurs structural deformation in the host lattice of $CdS/Zn_3(PO_4)_2$ and it introduce interface states. While comparing the reflectance spectra of (0.3, 0.6, 0.9 mol%) Mn^{2+} doped $CdS/Zn_3(PO_4)_2$ with that of pure $CdS/Zn_3(PO_4)_2$ exhibit similar features but slightly shifted to longer wavelength regions (red shifted) with decreasing energy from 2.48 to 2.434 eV indicating the quantum confinement effect.

This small variation in the energy bandgap reveals that there is a direct energy transfer between the valance electrons (sp) of CdS/Zn_3 $(PO_4)_2$-host lattice and 3d levels of the Mn^{2+} ions [14].

Table 4. Variation of Band gap of pure $CdSZn_3(PO_4)_2$ and Mn^{2+} doped $CdSZn_3(PO_4)_2$ nanocomposites obtained from Kulbeka-Munk equation.

Sample code	Variation of MnO dopingconcentration	Bandgap (eV)
Mn_0	0	2.480
Mn_1	0.3%	2.464
Mn_2	0.6%	2.451
Mn_3	0.9%	2.434

This shift in the band gap feature demonstrates excitation of electrons from the valence band to conduction band even under irradiation with visible light photons. This is advantageous for getting an increased PEC performance from a UV-active material. This study confirms that the incorporation of an optimal concentration of Mn^{2+} ions in $CdS/Zn_3(PO_4)_2$ may be beneficial material to offer an effective solar light absorption optical system, which may be used for the solar energy applications.

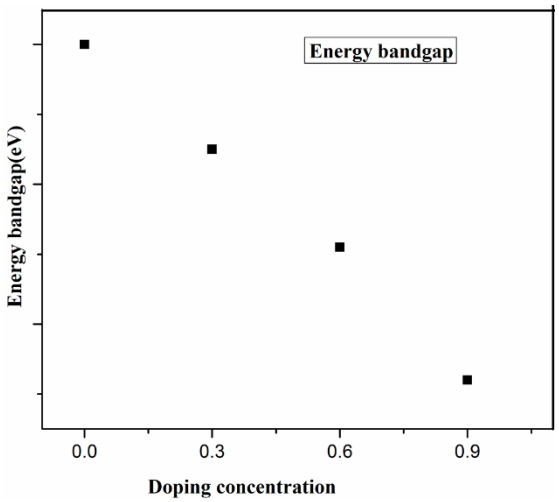

Fig. 7. Variation of energy bandgap with increasing Mn^{2+} doping concentration

3.2.2. Photoluminescence

Photoluminescence mechanism of pure and Mn^{2+} doped $CdSZn_3(PO_4)_2$ semiconductor nanocomposites were analyzed to understand the luminescence efficiency and their utilization for future optoelectronic applications.

Photoluminescence measurements of pure and Mn^{2+} doped $CdSZn_3(PO_4)_2$ nanocomposites were carried out with excitation wavelength 320 nm under room temperature and obtained PL spectra are shown in Fig. 8 (a) & 8 (b).

In case of undoped nanocomposite it shows a broad and intense peak originated in the visible region of wavelength 490 nm-600 nm. With effect of Mn^{2+} ions in the host lattice, the single broad emission peak shifted as multiple emission peaks in the Visible region of 360-650 nm and shows quantum confinement. The exciton (or) band edge emission occurs due the conduction electron of host lattice is trapped by deep trap centers or surface states; when the manganese exist in the host lattice the energy of these trapped electrons transferred to doped ions through exchange interaction process. This internal emission mechanism indicates the Mn^{2+} ions influence the luminescence behavior.

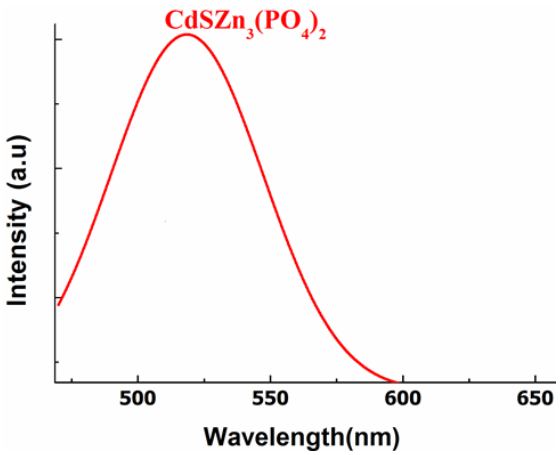

(a)

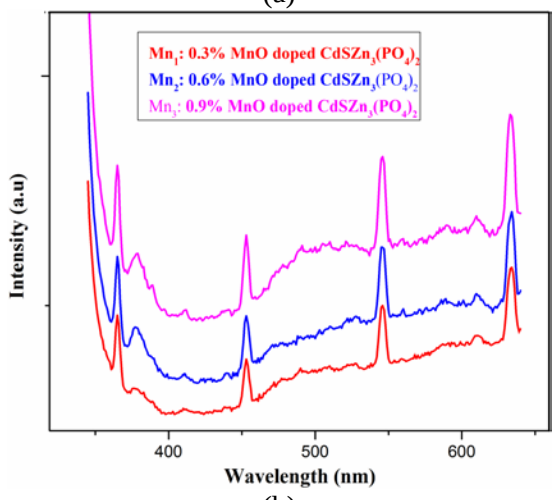

(b)

Fig. 8. a) PL spectra of pure $CdSZn_3(PO_4)_2$ nanocomposite b) PL spectra for (0.3%, 0.6% and 0.9%) Mn^{2+} doped $CdSZn_3(PO_4)_2$ nanocomposites.

The first strong luminescence peak at 365 nm occurs due to electron–hole recombination CdS. Due to excitonic or band edge emission of CdS second peak obtained around 455 nm exhibits blue emission. Another two more emission peaks at the position of 545 nm and 634 nm exhibit green and red emissions due to surface trap induced emission.

Photon energy will be transferred from the CdS host conduction band to the excited charge carriers trapped in shallow trap states after excitation. These trapped charge carriers have a d-d ($^4T_1 \rightarrow {}^6A_1$) transition of the tetrahedrally coordinated Mn^{2+} states, and there is a minor change in the peak location with increasing Mn doping concentration, which might be attributable to surface defects. As a result, the luminescence bands may be linked to donor, acceptor, and surface state transitions [15-18].

Fig. 9 shows the CIE (International Commission on Illu-mination) chromacity diagram of $CdS/Zn_3(PO_4)_2$-undoped and $CdSZn_3(PO_4)_2$-(0.3, 0.6 and 0.9 mol%) Mn^{2+} doped nanocomposites.

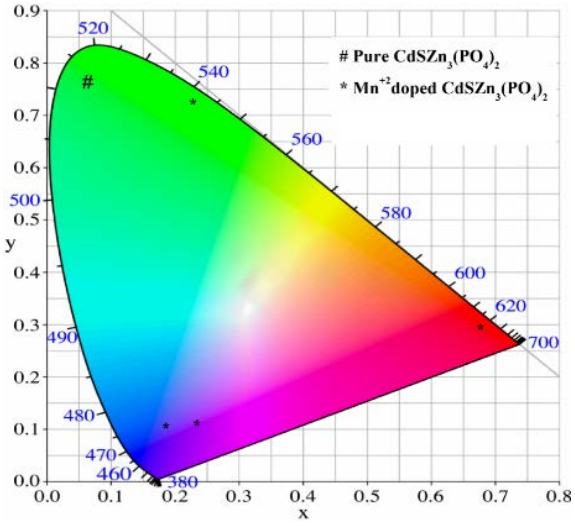

Fig. 9. CIE diagram of CdSZn3(PO4)2 and (0.3%, 0.6% and 0.9%) Mn2+ doped CdSZn3(PO4)2 nanocomposites

Table 5. Shifting of peak position in PL spectra with doping concentration ion in $CdSZn_3(PO_4)_2$ and (0.3%, 0.6% and 0.9 mol%) mn^{2+} doped $CdSZn_3(PO_4)_2$ nanocomposites.

Sample Code	Variation of Mn^{+2} concentration	PLpeak position I (λnm)	PL peak position II (λnm)	PL peak position III (λnm)	PL peak position IV (λnm)
Mn_0	0	518	-	-	-
Mn_1	0.3%	365	453	545	633
Mn_2	0.6%	366	455	548	635
Mn_3	0.9%	368	457	550	636

Table 6. Calculated Wavelength, color coordinates, CCT values from PL Spectra of pure$CdSZn_3(PO_4)_2$ and (0.3%, 0.6% and 0.9 mol%) Mn^{2+} doped $CdSZn_3(PO_4)_2$ nanocomposites.

Sample Code	Wavelength (nm)	Color Coordinates		CCT (K)
		x	y	
Mn_0	518	0.0899	0.7724	8879
Mn_1	365	0.28205	0.00525	3445
	453	0.2243	0.01500	2513
	545	0.2657	0.7243	6416
	633	0.71172	0.28823	7307
Mn_2	364	0.28123	0.00536	3862
	453	0.2216	0.01583	2460
	545	0.2685	0.7198	6385
	634	0.71256	0.28856	7299
Mn_3	365	0.28256	0.00534	3899
	452	0.2276	0.01562	2562
	543	0.2688	0.7194	6381
	632	0.71262	0.28849	7306

To characterize color of emission of prepared nanocomposites CIE parameters such as color coordinates (X, Y) and the colour correlated temperature (CCT) values are estimated. By using Colour calculator software colour coordinates were determined. To know the quality of the emitted light (Color Correlated Temperature) values have been calculated from color coordinates using McCamy empirical formula [19, 20].

$CCT = -437n^3 + 3601n^2 - 6861n + 5514:31$

Where $n = (x-x_e)/(y-y_e)$ and the chromaticity epicenter is at $x_e = 0.3320$ and $y_e = 0.1858$, (x, y) are the calculated color coordinates of nanocomposite.

From the CIE diagram (Fig. 9), it has been observed that Colour coordinates shows a wide range from blue to red region with doping of Mn^{2+} ions in the host lattice of $CdSZn_3(PO_4)_2$. The Colour correlated temperature of the synthesized phosphors were found in the range of 2513– 7307 K. In general, CCT value greater than 5000 K suitable for cold white emission. From the CIE analysis Mn^{2+} doped of $CdSZn_3(PO_4)_2$ nanocomposites are suitable for solid state lighting applications [21].

4. CONCLUSIONS

Undoped $CdSZn_3(PO_4)_2$ and mn^{2+} (0.3, 0.6 and 0.9 mol%) doped $cdszn_3(po_4)_2$ nanocomposite semiconductors were prepared by a hydrothermal method. From xrd results mn^{2+} doped $cdszn_3(po_4)_2$ shows both cds-hexagonal structure and $zn_3(po_4)_2$ monoclinic structure. With influence of mn^{2+} ions in the host lattice there occurs a lattice distortion that cause phase change of γ-phase of $zn_3(po_4)_2$ to β-phase of $zn_3(po_4)_2$ without disturbing the CdS-hexagonal phase. Average crystallite size of synthesized nanocomposites are found in the range of 22-25 nm and also estimated lattice strain, dislocation density to understand internal distortion of the samples. The molecular vibrations and functional groups presented in the samples are analyzed by ft-ir spectrum. Surface morphology of the nanocomposites represents hexagonal spheres on the rectangular flakes and with increasing of mn2+ ion concentration the interatomic distance between the hexagonal spheres decreases and forms a rod like structure on the flakes. Edax results confirm the chemical composition according to stoichiometry of the samples. With the increase in the mn^{2+} ions concentration in the host lattice optical energy bandgap decreases indicates the quantum confinement of synthesized samples. Photoluminescence results shown shallow trapped states due to tetrahedrally coordinated mn^{2+} states related d-d (4t1→ 6a1) transition and with influence of mn^{2+} ions exhibiting multiple peaks in the uv-visible region (365- 634 nm) emitting rgb (red, green, blue) luminescence. The colour correlated temperatures of the synthesized phosphors were found in the range of 2513– 7307 k. In general, cct value above 5000 k suitable for cold white emission. From the cie analysis mn^{2+} doped of $cdszn_3(po_4)_2$ nanocomposites are suitable for solid state lighting applications.

REFERENCES

[1] N. H. Patel, M. P. Deshpande, S. V. Bhatt, K. R. Patel, S. H. Chaki, Structural and magnetic properties of undoped and Mn-doped CdS nanoparticles prepared by chemical co-precipitation method. Adv Mater Lett, 2014, 5, 671–677. https://doi.org/10.5185/AMLETT.2014.1574.

[2] B. Grzmil, B. Kic, K. Lubkowski, studies on obtaining of zinc phosphate nanomaterials. Rev. Adv. Mater. Sci. 14, 46–48 (2007).

[3] T. Maldiney, A. Bessiere, J. Seguin, E. Teston, S. K. Sharma, B. Viana, A. J. J. Bos, P. Dorenbos, M. Bessodes, D. Gourier, D. Scherman, C. Richard, The in vivo activation of persistent nanophosphors for optical imaging of vascularization, tumours and grafted cells. Nat. Mater, 2014, 13, 418–426. https://doi.org/10.1038/nmat3908.

[4] Yoffe, Abraham D. "Semiconductor quantum dots and related systems: electronic, optical, luminescence and related properties of low dimensional systems." Advances in physics, 2001, 50, 1-208. https://doi.org/10.1080/00018730010006608.

[5] Wang, Feifan, Qi Li, and Dongsheng Xu. "Recent progress in semiconductor-based nanocomposite photocatalysts for solar-to-chemical energy conversion." Advanced Energy Materials, 2017, 7, 1700529.

https://doi.org/10.1002/aenm.201700529.

[6] Ouendadji, S., S. Ghemid, H. Meradji, and F. El Haj Hassan. "Theoretical study of structural, electronic, and thermal properties of CdS, CdSe and CdTe Compounds." Computational Materials Science, 2011, 50, 1460-1466. https://doi.org/10.1016/j.commatsci.2010.11.035.

[7] Yuvaraj, S., Alison Christina Fernandez, M. Sundararajan, Chandra Sekhar Dash, and P. Sakthivel. "Hydrothermal synthesis of ZnO–CdS nanocomposites: structural, optical and electrical behavior." Ceramics International, 2020, 46, 391-402. https://doi.org/10.1007/s10948-020-05665-1.

[8] Muswareen, SK Khaja, M. Subba Rao, G. Sridevi, and Sandhya Cole. "Sol-gel synthesis of pure and TiO_2 doped $CdOFePO_4$ nanocomposites and investigation of their structural and optical properties." Materials Science in Semiconductor Processing, 2019, 102, 104588. https://doi.org/10.1016/j.mssp.2019.104588.

[9] Dong, Jing-Jing, Chun-Yang Zhen, Hui-Ying Hao, Jie Xing, Zi-Li Zhang, Zhi-Yuan Zheng, and Xing-Wang Zhang. "Controllable synthesis of ZnO nanostructures on the Si substrate by a hydrothermal route." Nanoscale research letters, 2013, 8, 1-7. https://doi.org/10.1186/1556-276X-8-378.

[10] Liang, Yuan-Chang, and Tsai-Wen Lung. "Growth of hydrothermally derived CdS-based nanostructures with various crystal features and photoactivated properties." Nanoscale Research Letters, 2016, 11, 1-11. https://doi.org/10.1186/s11671-016-1490-x.

[11] Chander, H., Development of nanophosphors-A review. Mater. Sci. Eng. R Rep. 2005, 49, 113-155, https://doi.org/10.1016/j.mser.2005.06.001.

[12] Fang, Xiaosheng, Limin Wu, and Linfeng Hu. "ZnS nanostructure arrays: a developing material star." Advanced Materials, 2011, 23, 585-598. https://doi.org/10.1002/adma.201003624.

[13] Christy, Alfred A., Olav M. Kvalheim, and Rance A. Velapoldi. "Quantitative analysis in diffuse reflectance spectrometry:a modified Kubelka-Munk equation." VibrationalSpectroscopy, 1995, 9, 19-27. https://doi.org/10.1016/0924-2031(94)00065-O.

[14] Thao, Nguyen Thu, Ho Nhat Phuong, Ha Thanh Tung, Nguyen Tan Phat, Huynh Thanh Dat, and Lam Quang Vinh. "The enhanced current density of the quantum dots solar cells based on CdSe: Mn^{2+} crystalline." Optical Materials, 2018, 84, 199-204. https://doi.org/10.1016/j.optmat.2018.06.069.

[15] Chen, Weiwei, Yangang Sun, Jianhua Ge, Fengge Song, Yu Xie, Yuanyuan Zheng, and Pinhua Rao. "Synthesis and enhanced photocatalytic activity of the flower-like $CdS/Zn_3(PO_4)_2$Z-scheme heteronanostructures." CrystEngComm, 2021, 23, 8291-8300. https://doi.org/10.1039/D1CE01007G.

[16] Ganguly, A., and S. S. Nath. "Mn-doped CdS quantum dots as sensitizers in solar cells." Materials Science and Engineering: B, 2020, 255, 114532. https://doi:10.1016/j.mseb.2020.114532.

[17] Elias, Md, Sonia Akter, Md Awlad Hossain, and Mahmudul Hassan Suhag. "Fabrication of $Zn_3(PO_4)_2$/carbon nanotubes nanocomposite thin film via sol-gel drop coating method with enhanced photocatalytic activity." Thin Solid Films, 2021, 717, 138472. https://doi.org/10.1016/j.tsf.2020.138472.

[18] Sreedevi, G., S. K. Muswareen, V. Jayalakshmi, and Sandhya Cole. "Effect of TiO_2 doping on structural and optical properties of $CdSZn_3(PO_4)_2$ nanocomposites." Applied Physics A, 2019, 125, 1-11. https://doi.org/10.1007/s00339-019-3037-3.

[19] Al-Hussam, Abdullah MA, and Salah Abdul-Jabbar Jassim. "Synthesis, structure, and optical properties of CdS thin films nanoparticles prepared by chemical bath technique." Journal of the Association of Arab Universities for Basic and Applied Sciences, 2012, 11, 27-31. https://doi.org/10.1016/j.jaubas.2011.10.001.

[20] Stella, R. Joyce, G. Thirumala Rao, V. Pushpa Manjari, B. Babu, Ch Rama Krishna, and R. V. S. S. N.

Ravikumar. "Structural and optical properties of CdO/ZnS core/shell nanocomposites." Journal of Alloys and Compounds, 2015, 628 39-45. https://doi.org/10.1016/j.jallcom.2014.11.201.

[21] Anikeeva, Polina O., Jonathan E. Halpert, Moungi G. Bawendi, and Vladimir Bulovic. "Quantum dot light-emitting devices with electroluminescence tunable over the entire visible spectrum." Nano letters, 2009, 9, 2532-2536. https://doi.org/10.1021/nl9002969.